

A pilot ASKAP survey for radio transients towards the Galactic Centre

Ziteng Wang,^{1,2,3}★ Tara Murphy,^{1,3} David L. Kaplan,⁴ Keith W. Bannister,² Emil Lenc,² James K. Leung,^{1,2,3} Andrew O’Brien,⁴ Sergio Pintaldi,⁶ Joshua Pritchard,^{1,2,3} Adam J. Stewart,¹ Andrew Zic,^{5,2}

¹*Sydney Institute for Astronomy, School of Physics, University of Sydney, Sydney, New South Wales 2006, Australia.*

²*CSIRO, Space and Astronomy, PO Box 76, Epping, New South Wales 1710, Australia*

³*ARC Centre of Excellence for Gravitational Wave Discovery (OzGrav), Hawthorn, Victoria, Australia*

⁴*Center for Gravitation, Cosmology, and Astrophysics, Department of Physics, University of Wisconsin-Milwaukee, P.O. Box 413, Milwaukee, WI 53201, USA*

⁵*Department of Physics and Astronomy, and Research Centre in Astronomy, Astrophysics and Astrophotonics, Macquarie University, NSW 2109, Australia*

⁶*Sydney Informatics Hub, The University of Sydney, NSW 2008, Australia*

Accepted XXX. Received YYY; in original form ZZZ

ABSTRACT

We present the results of a radio transient and polarisation survey towards the Galactic Centre, conducted as part of the Australian Square Kilometre Array Pathfinder Variables and Slow Transients pilot survey. The survey region consisted of five fields covering $\sim 265 \text{ deg}^2$ ($350^\circ \lesssim l \lesssim 10^\circ$, $|b| \lesssim 10^\circ$). Each field was observed for 12 minutes, with between 7 and 9 repeats on cadences of between one day and four months. We detected eight highly variable sources and seven highly circularly-polarised sources (14 unique sources in total). Seven of these sources are known pulsars including the rotating radio transient PSR J1739–2521 and the eclipsing pulsar PSR J1723–2837. One of them is a low mass X-ray binary, 4U 1758–25. Three of them are coincident with optical or infrared sources and are likely to be stars. The remaining three may be related to the class of Galactic Centre Radio Transients (including a highly likely one, VAST J173608.2–321634, that has been reported previously), although this class is not yet understood. In the coming years, we expect to detect ~ 40 bursts from this kind of source with the proposed four-year VAST survey if the distribution of the source is isotropic over the Galactic fields.

Key words: radio continuum: transients – Galaxy: centre – radio continuum: stars

1 INTRODUCTION

Many types of sources exhibit variability at radio wavelengths, including pulsars, supernovae, flaring stars and X-ray binaries. The variable radio emission from these sources is often associated with high-energy astrophysical phenomenon. Studying the properties of variable sources can help us understand the physical mechanisms that cause them, as well as the properties of their local environments (Fender et al. 2015). Radio transients surveys also allow us to discover new types of objects. For example, Hyman et al. (2005) discovered Galactic Centre Radio Transients (GCRTs), an unknown class of transient radio sources, in a search for transient and variable sources with the Very Large Array (VLA).

The Galactic Centre (GC) is a promising region for finding transient or variable radio sources (e.g., Hyman et al. 2003). The GC is inhabited by stars, white dwarfs, neutron stars and stellar mass black holes, or even those objects in binary systems (e.g., Kassim et al. 2003). Some of them are known to be variable or transient at radio wavelengths, such as flaring stars, pulsars and low-mass X-ray binaries (e.g., Fender et al. 2015). X-ray observations also support the case for searching for transient radio sources towards the GC. Skinner (1993) reported that the X-ray source density peaked towards the GC and Munro et al. (2003) found ~ 2000 hard X-ray sources near the

GC; some of them likely associated with neutron stars. We therefore expect a concentration of radio transients towards the GC.

There have only been a few dedicated radio transient searches towards the GC, but these searches have found a number of transients. For example, Hyman et al. (2002, 2003, 2005, 2009) searched for radio transients at 330 MHz toward the GC with the VLA and found three unclassified objects that they called GCRTs. Chiti et al. (2016) searched for short timescale transients in archival VLA data and found two transient (but possibly spurious) sources without convincing explanations. Zhao et al. (2020) detected 82 variable or transient Galactic centre compact radio sources and argued that some of the sources may be undiscovered pulsars.

Some transient and variable sources are known to be circularly polarised. Flaring stars can give off circular polarised emission by plasma emission or electron cyclotron maser emission (e.g., Lynch et al. 2017). Pulsars can emit circular polarised emission (e.g., Johnston & Kerr 2018) but the origin remains unclear (e.g., Radhakrishnan & Rankin 1990; Melrose & Luo 2004). Roy et al. (2010) found that bursts from GCRT J1745–3009 can reach as high as 100 per cent circular polarisation. In contrast, fewer than 0.1 per cent of radio sources are circularly polarised at more than a few per cent of their total intensity, which makes it easier to find polarised sources (e.g., Lenc et al. 2018), especially in crowded regions. Previous polarisation searches have identified new sources, including a new millisecond pulsar (PSR J1431–6328; Kaplan et al. 2019), the first brown dwarf discovered at radio wavelengths (Vedantham et al.

★ E-mail: zwan4817@uni.sydney.edu.au

2020), and previously undetected flaring stars (Pritchard et al. 2021; Callingham et al. 2021).

The Australian Square Kilometre Array Pathfinder (ASKAP; Johnston et al. 2008; Hotan et al. 2021) was designed as a rapid wide-field survey instrument. It is a radio interferometer with a wide field-of-view ($\sim 30 \text{ deg}^2$) and its sensitivity can reach a typical rms of 0.24 mJy in a 12 min integration. ASKAP’s wide field-of-view and high instantaneous sensitivity improve the effectiveness for transient surveys, notably the ASKAP survey for Variables and Slow Transients (VAST; Murphy et al. 2013, 2021). VAST will investigate the dynamic radio sky on timescales from seconds to months. During 2019–2020, VAST was allocated 100 hours observing time to conduct a Phase I of the Pilot Survey (VAST-P1; Murphy et al. 2021). VAST-P1 consists of six survey regions covering 5131 deg^2 . Observations for VAST-P1 commenced in mid-2019 and finished in mid-2020. In this paper, we present the results from the Pilot Survey searching for variable and circularly polarised sources in the low Galactic latitude region (see Figure 1). In §2, we describe the observations and check the data quality; in §3, we present the methods for searching variable and circular polarised sources and we summarize the details for all the candidates; and in §4, we discuss the candidates from our searches.

2 OBSERVATIONS AND QUALITY CHECKS

In this paper, we used the data from two ASKAP surveys: the Rapid ASKAP Continuum Survey low (RACS-low; McConnell et al. 2020) and VAST-P1. Both surveys were conducted at a central frequency of 887.5 MHz with a bandwidth of 288 MHz. All four instrumental polarisation products (XX, XY, YX, and YY) were recorded for both surveys to allow images to be made in four Stokes parameters (I, Q, U, and V). We used *combined* images in our search to improve the sensitivity in the overlapped regions. *Combined* images are made by mosaicking the individual field images together per epoch (see Murphy et al. 2021 for details). The VAST-P1 survey incorporates RACS-low as its first epoch, and we therefore refer to RACS-low as “epoch 00” in this paper. We used the SELAVY source finding software (Whiting & Humphreys 2012) with its default settings to produce source catalogues for the images. SELAVY models source components with 2D Gaussians. The uncertainty for flux density measurements is based on the uncertainty in the Gaussian fitting and the local noise.

2.1 RACS-low

There are five tiles near the Galactic Centre in RACS-low: 1724–31A, 1739–25A, 1752–31A, 1753–18A and 1806–25A. The median RMS noise of these five tiles was $\sim 0.36 \text{ mJy/beam}$, which is higher than the typical noise of RACS-low due to the bright and diffuse emission near the Galactic Centre. The observations were conducted between 2019 April 25 and 2019 April 28.

We used the early processing RACS-low data in this paper. Further improvements have been applied to the published RACS-low images and source catalogues. A detailed discussion is in McConnell et al. (2020) and Hale et al. (2021).

We performed quality checks of the astrometric accuracy and flux density scale for the pre-release RACS-low data. We extracted bright

($\text{SNR} \geq 7$), compact¹ sources with SELAVY that are isolated by a minimum of 150 arcsec from other sources. These sources have low positional errors ($\lesssim 1.5 \text{ arcsec}$), are less likely to be spurious detections or artefacts, and are free from contamination from close neighbours, which enables us to get a robust astrometry and flux density scale comparison. We then crossmatched them with bright compact isolated sources (1145 sources within low Galactic latitude region) in the published RACS catalogue (Hale et al. 2021). There were 482 sources matched using a 10 arcsec crossmatch radius. The median and standard deviation of the positional offsets are $0.01 \pm 1.02 \text{ arcsec}$ in right ascension and $-0.12 \pm 0.90 \text{ arcsec}$ in declination (see Figure 2). The flux density ratio is 1.05 with a standard deviation of 0.12 (see Figure 3).

2.2 VAST-P1

VAST-P1 uses the same tiling footprint, frequency, and bandwidth as RACS-low. There are 13 epochs in total for VAST-P1, but seven of them only have partial coverage of the full survey footprint (see Murphy et al. 2021 for details). There are five VAST-P1 tiles covering $\sim 265 \text{ deg}^2$ near the Galactic Centre region. Each tile was observed with an integration time of $\sim 12 \text{ min}$. The median RMS noise of the five tiles we used is $\sim 0.39 \text{ mJy/beam}$. All observations were processed using standard procedures in the ASKAPSOFT package (Cornwell et al. 2016; Guzman et al. 2019) and SELAVY (Whiting & Humphreys 2012) was used for source finding and flux measurement.

We performed the quality checks on VAST-P1 data for the Galactic Centre region in the same way as for the pre-release RACS-low data. The observation for field 1724–31A in epoch 09 had poor calibration, which resulted in astrometry errors and reduced flux densities, and so we excluded this observation in the rest of our analysis. All nine epochs have a median VAST-P1/RACS-low flux density ratio between 0.96 and 1.06 (within 10 per cent, see Figure 3). The overall ratio is 1.03 with a 1σ scatter of 0.15. In our analysis, we selected variability thresholds such that the overall flux variation between epochs is not significant (see Section 3.1). The astrometric accuracy for VAST-P1 is shown in Figure 2. The median and standard deviation of the positional offsets are $0.15 \pm 1.20 \text{ arcsec}$ in right ascension and $0.04 \pm 1.22 \text{ arcsec}$ in declination. We note that the offset for epoch 03 was larger compared to other epochs, but still within a single image pixel ($< 2.5 \text{ arcsec}$).

3 SEARCH METHODOLOGY

3.1 Variable Search

We performed a search for variable sources using the VAST pipeline (Murphy et al. 2021; Pintaldi et al. 2021). For a given source, in an epoch in which it was not detected, we used the synthesized beam of that epoch to perform forced fitting at the source position to get a *forced* measurement. We found 46 732 unique sources in all fields and epochs. We excluded 6 776 sources with only one measurement (most of such sources appear in the RACS-low footprint, but not the VAST footprint, see Figure 1) and 12 637 sources that were only detected in one epoch (but with > 1 measurement) but had an $\text{SNR} < 7.0$ to avoid false detections. This resulted in 29 410 unique sources to analyse for variability. We used the modulation index (V) to measure the degree of variability, and the reduced chi-square (η) statistic to

¹ Compactness follows the definition by Hale et al. (2021) of an integrated to peak flux ratio of $S_I/S_P < 1.024 + 0.69 \times \text{SNR}^{-0.62}$.

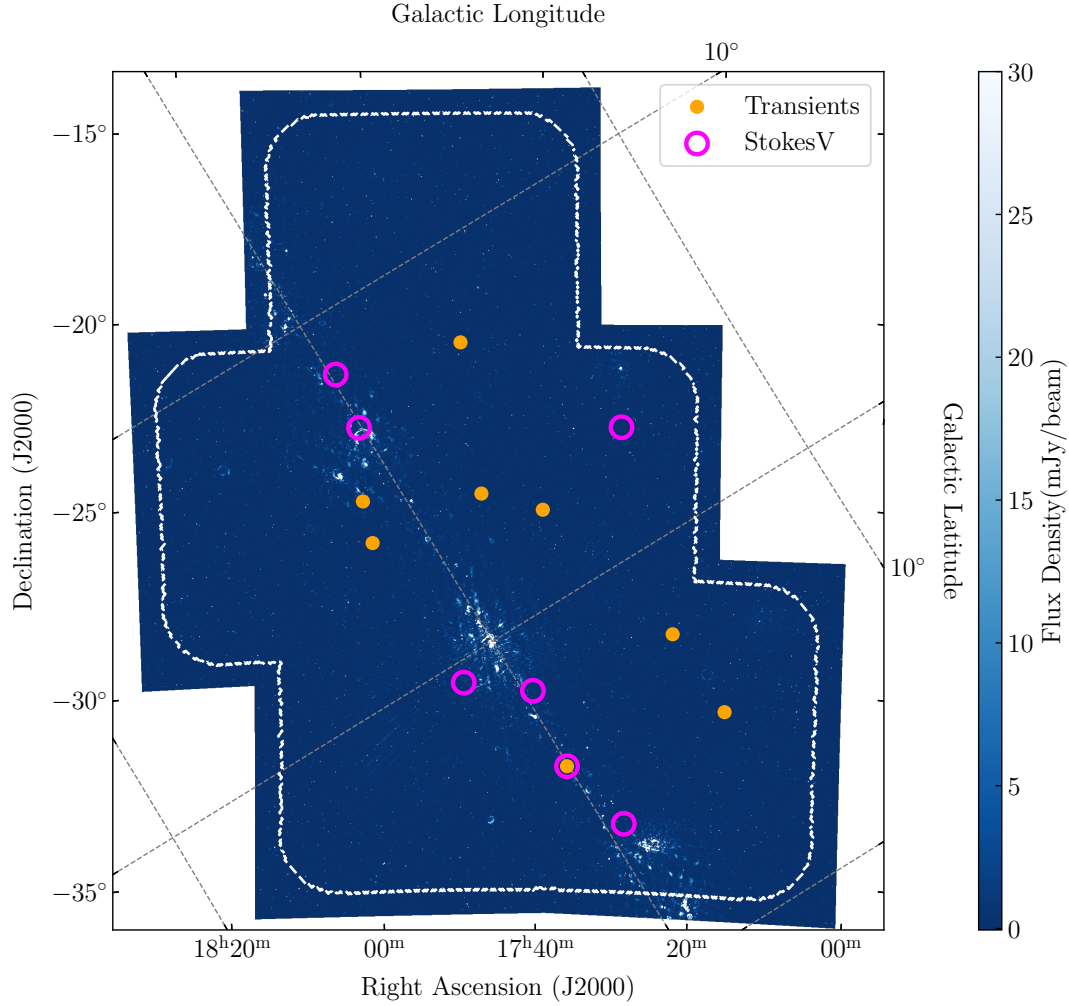


Figure 1. A mosaicked image of the RACS-low Low Galactic Latitude region. White dashed line shows the boundary of VAST Low Galactic Latitude region. Due to lack of neighboring fields, the VAST coverage is smaller than RACS-low though they share the same footprint. A grid of Galactic coordinates is shown in grey dashed lines. The transient and circularly polarised (Stokes V) sources we found are shown as blue circles and magenta hollow circles, respectively.

show the significance of the measured variability (Rowlinson et al. 2019). They are defined as

$$V = \frac{\sigma_S}{\bar{S}} \quad (1)$$

$$\eta = \frac{1}{N-1} \sum_{i=1}^N \frac{(S_i - \bar{S}_{wt})^2}{\sigma_i^2} \quad (2)$$

where S_i is the flux density in epoch i , \bar{S} is the mean flux density, σ_i is the detection uncertainty, and \bar{S}_{wt} is the weighted mean flux density which is given by

$$\bar{S}_{wt} = \frac{\sum_{i=1}^n (S_i / \sigma_i^2)}{\sum_{i=1}^n (1 / \sigma_i^2)} \quad (3)$$

Before determining the variability thresholds, we excluded extended sources and sources likely to be artefacts by removing sources that satisfied any of the following criteria:

- The source was extended (the ratio of integrated flux to peak flux > 1.5);
- The source contained multiple components;

- The source was close to other sources (separation < 30 arcsec, which is about two times the size of the point spread function for VAST-P1);

- The source was close to the edges of the image ($< 2^\circ$, where the typical rms is much higher, ~ 1.5 mJy, compared to the image centre).

When calculating the thresholds, we excluded outliers (using a 3σ threshold) and fit the η and V distributions with Gaussians in logarithmic space (Rowlinson et al. 2019) to calculate the means (μ) and standard deviations (σ). We used a 2σ (i.e.: $\mu + 2\sigma$) threshold to select our candidates ($V > 0.44$, $\eta > 6.23$). The 2σ threshold enabled us to pick sources that are highly variable and also makes the number of candidates manageable for manual inspection (see Murphy et al. 2021). This resulted in 35 sources in our candidate space, as shown in the η - V plot in Figure 4.

After manually inspecting images and lightcurves for the 35 candidates, we found eight variable sources (see Table 1). Jupiter moved across the field of view in one observation and was identified as a variable (green star in Figure 4). The other candidates were rejected because they were coincident with either imaging artefacts or components with extended sources. The lightcurves of the eight variable

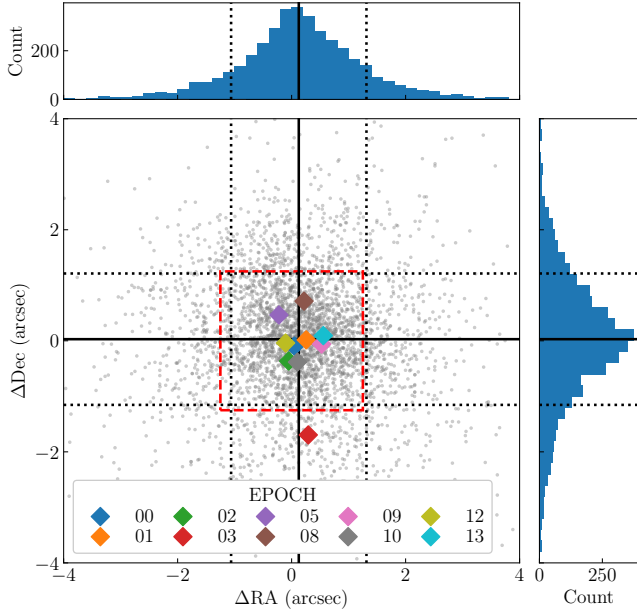


Figure 2. Astrometric accuracy for bright compact isolated sources in region 5 of pre-release RACS-low (epoch 00) and VAST-P1 compared to sources from the published RACS catalogue. Red dashed box shows the image pixel size (2.5×2.5 arcsec). The offsets for each matched pair are shown in gray circles. We show the median offset for each epoch as coloured diamonds.

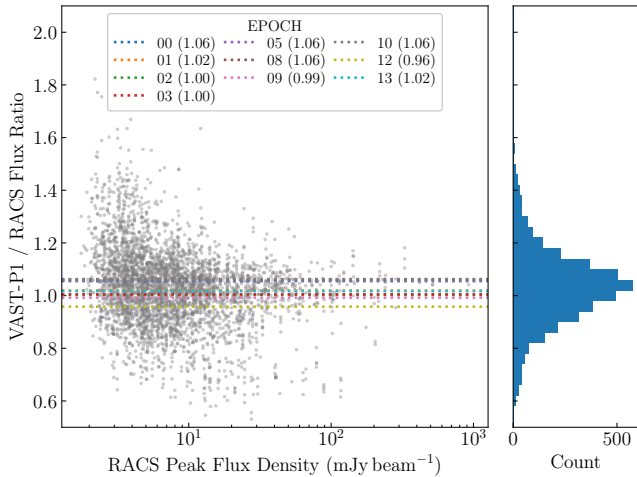


Figure 3. Flux density scale comparison for sources in region 5, comparing those measured in pre-release RACS-low (epoch 00) and VAST-P1 to RACS. We show the median ratio for each epoch as dotted lines. The ratios for each matched pair are shown in gray circles. The overall median ratio is 1.03 with a scatter of 0.15.

sources are presented in Figure 5. We analyse each of these sources in §4. The variability statistics and the properties of the sources are listed in Table 1.

3.2 Polarisation Search

We also performed a search for circularly polarised sources using the method described by Pritchard et al. (2021). We used SELAVY with default setting for source finding and flux measurement in the Stokes V images. We extracted 1 835 positive components from the

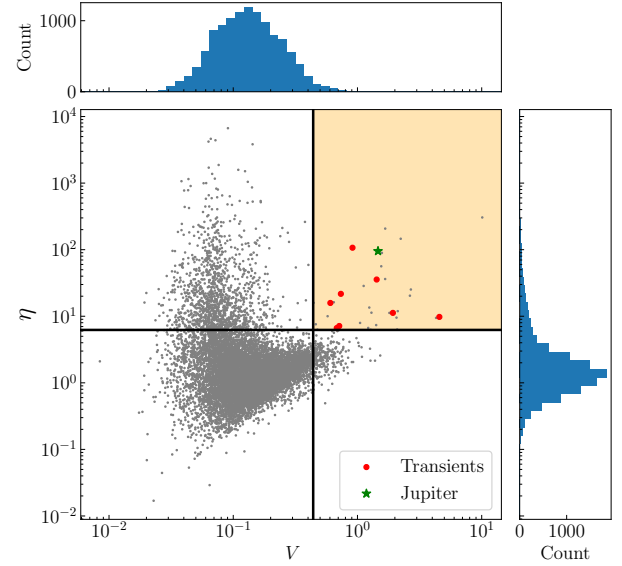


Figure 4. Transient phase-space (η - V) plot for all sources. Red dots show the variable sources detected in our analysis and the green star shows the Jupiter detected in the survey by chance. Black lines represent the minimum threshold of variability statistics (vertical line: $V = 44.0\%$ and horizontal line: $\eta = 6.23$) we used among fields. The gray dots show the sources that does not meet our selection criteria or were ruled out by manual inspection.

normal images and 2 443 negative components from the inverted images. We crossmatched the combined 4 278 components against the Stokes I components using a radius of 15 arcsec, to identify the corresponding component in Stokes I. We searched for compact polarised sources only, so we excluded extended components (the ratio of integrated flux to peak flux > 1.5) and components with siblings. We crossmatched all components in different epochs again using a 15 arcsec crossmatch radius which resulted in 1 740 unique sources and we selected 95 sources with fractional polarisation $f_p = |V|/I$ greater than 6 per cent for manual inspection. The threshold we chose is 10 times the median circular polarisation leakage in RACS-low (~ 0.6 per cent, see Pritchard et al. 2021) to minimise the possibility of selecting leakage in our sample.

Figure 6 shows all highly circular polarised sources we found. Five of them were identified as known pulsars, six sources are associated with leakage from bright Stokes I sources (all six sources are at the edge of the *combined* image, where the leakage is expected to be higher, see e.g., Pritchard et al. 2021), and there are two unclassified sources with no known pulsars or stars matched (we show the details in Table 1). All other sources (the grey crosses in Figure 6) were either imaging artefacts caused by leakage of the bright Stokes I sources or associated with extended Stokes I sources such as radio galaxies, planetary nebula and an H II region.

4 RESULTS

We found eight highly variable sources in the transient search and seven highly circular-polarised sources in the polarisation search. Together they resulted in 14 unique sources in total.

For each source, we searched for archival detections in previous radio surveys including the quick look images from the Karl G. Jansky Very Large Array Sky Survey (VLASS; Lacy et al. 2020), the TIFR GMRT Sky Survey (TGSS; Intema et al. 2017), the GaLac-

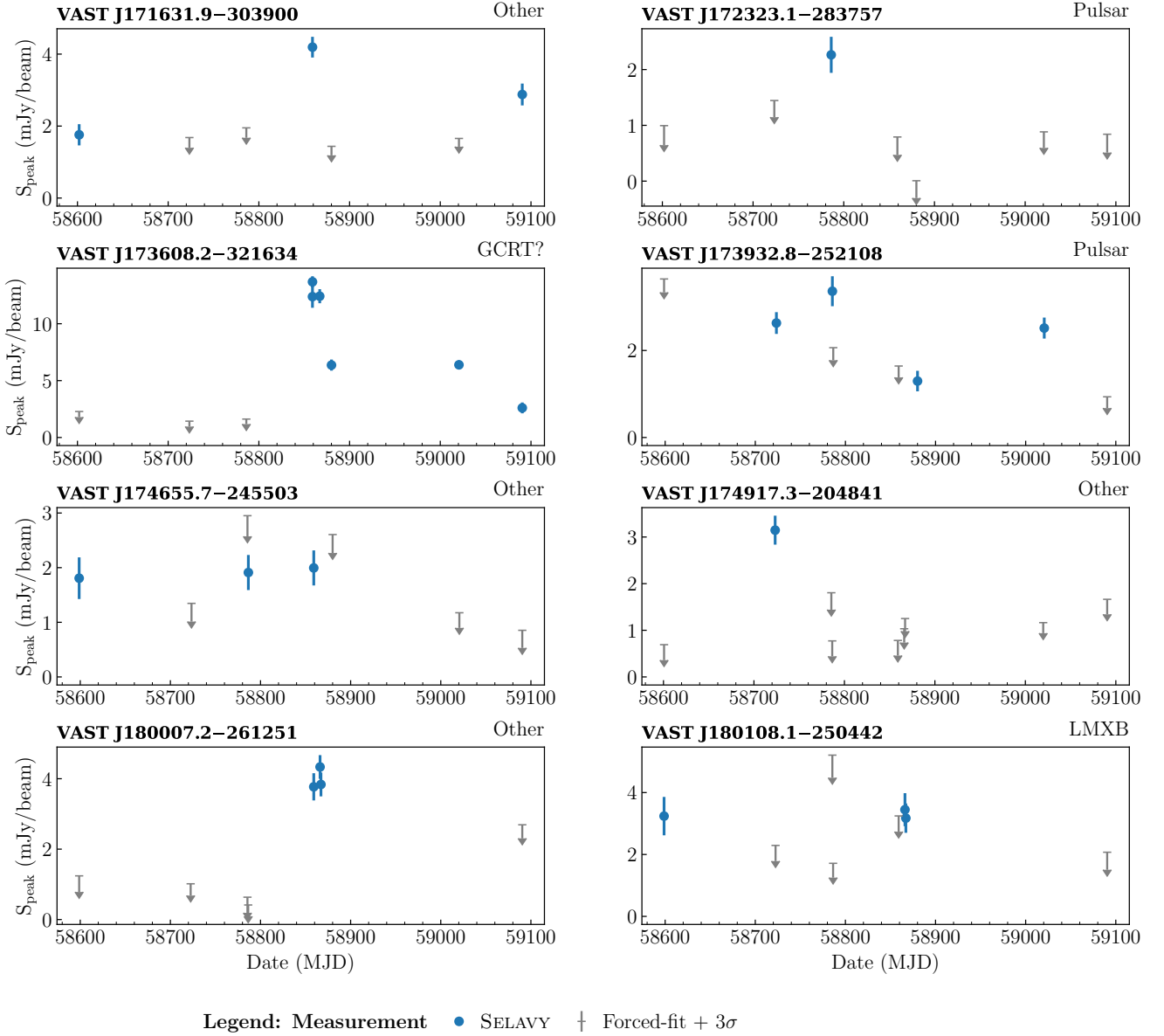


Figure 5. Lightcurves of the variables identified in VAST-P1 Low Galactic Latitude region. Blue circles are peak flux density measurements from SELAVY. Gray lines show the 3σ upper-limits of the forced-fitted flux density for images where there was no SELAVY detection.

tic and Extragalactic All-sky MWA (GLEAM; Wayth et al. 2015; Hurley-Walker et al. 2017), the NRAO VLA Sky Survey (NVSS; Condon et al. 1998) and the second epoch Molonglo Galactic Plane Survey (MGPS-2; Murphy et al. 2007). We also searched for optical or infrared counterparts in *Gaia* DR3 (Babusiaux et al. 2022), SkyMapper (Wolf et al. 2018; Onken et al. 2019), VISTA Variables in the Via Lactea (VVV; Minniti et al. 2010), the Wide-field Infrared Survey Explorer catalogue (WISE; Cutri & et al. 2012) and the Two Micron All Sky Survey (2MASS; Skrutskie et al. 2006). We discuss these sources individually below.

4.1 Pulsars

Two of our highly variable sources and five of our highly polarised sources are identified with known pulsars (Manchester et al. 2005², Kaplan 2022³). Pulsars are one of the most highly polarised radio source classes known (e.g., Lyne & Manchester 1988). Five pulsars (PSR J1740–3015, PSR J1803–2137, PSR J1801–2304, PSR J1730–2304, PSR J1749–3002) identified in our polarisation search do not appear to be remarkable, so we will not discuss them in detail. However, two of the pulsars we identified in the transient search are more interesting.

VAST J172323.1–283757 is identified as PSR J1723–2837, an

² The Australia Telescope National Facility Pulsar Catalogue: <https://www.atnf.csiro.au/research/pulsar/psrcat/>

³ Pulsar Survey Scraper: <https://pulsar.cgca-hub.org/>

Table 1. Highly variable and circularly polarised sources identified in the VAST-P1 Low Galactic Latitude region. The coordinate of each source is given as the weighted average of all SELAVY detections, where the weight is the inverse square of the positional error. σ_{pos} is the averaged positional uncertainty. η and V are the variability parameters described in the text. nE gives the number of epochs (observations) that cover the source location. nD gives the number of detections. $|V|/I$ is the ratio of Stokes V to Stokes I flux density measured in the epoch for which this is a maximum, or the most constraining 3σ upper limit in the case of non-detections in Stokes V. Method shows the way the source was selected.

Source Name	RA (J2000)	Dec (J2000)	σ_{pos} (")	η	V	nE	nD	S_{max} (mJy/beam)	$ V /I$	Method	ID
Pulsars											
VAST J172323.1–283757	17:23:23.1	−28:37:57	0.6	9.78	4.56	7	1	2.3±0.3	< 0.47	var	PSR J1723–2837
VAST J173021.7–230431	17:30:21.7	−23:04:31	0.5	28.66	0.19	8	8	12.4±0.4	0.19	cir	PSR J1730–2304
VAST J173932.8–252108	17:39:32.8	−25:21:08	0.6	15.84	0.60	8	4	3.4±0.3	< 0.32	var	PSR J1739–2521
VAST J174033.8–301542	17:40:33.8	−30:15:42	0.5	2.00	0.10	9	9	11.6±1.2	0.29	cir	PSR J1740–3015
VAST J174913.5–300235	17:49:13.5	−30:02:35	0.6	5.42	0.14	7	7	10.9±0.9	0.19	cir	PSR J1749–3002
VAST J180119.8–230444	18:01:19.8	−23:04:44	0.5	2.16	0.08	8	8	43.2±1.7	0.12	cir	PSR J1801–2304
VAST J180351.4–213706	18:03:51.4	−21:37:06	0.5	15.10	0.14	9	9	21.4±0.6	0.29	cir	PSR J1803–2137
Low Mass X-ray Binaries											
VAST J180108.1–250442	18:01:08.1	−25:04:42	0.6	6.65	0.68	8	3	3.4±0.5	< 0.32	var	4U 1758–25
Galactic Centre Radio Transients											
VAST J173608.2–321634	17:36:08.2	−32:16:34	0.5	107.00	0.91	9	6	13.7±0.5	0.41	var/cir	?
Other sources											
VAST J171631.9–303900	17:16:31.9	−30:39:00	0.6	21.70	0.74	7	3	4.2±0.3	< 0.26	var	Star?
VAST J172841.2–334548	17:28:41.2	−33:45:48	0.6	7.67	1.66	7	1	3.7±0.6	0.98	cir	–
VAST J174655.7–245503	17:46:55.7	−24:55:03	0.6	7.14	0.71	8	3	2.0±0.3	< 0.54	var	Star?
VAST J174917.3–204841	17:49:17.3	−20:48:41	0.5	11.24	1.93	9	1	3.1±0.3	< 0.35	var	–
VAST J180007.2–261251	18:00:07.2	−26:12:51	0.5	35.62	1.43	8	3	4.3±0.3	< 0.25	var	Star

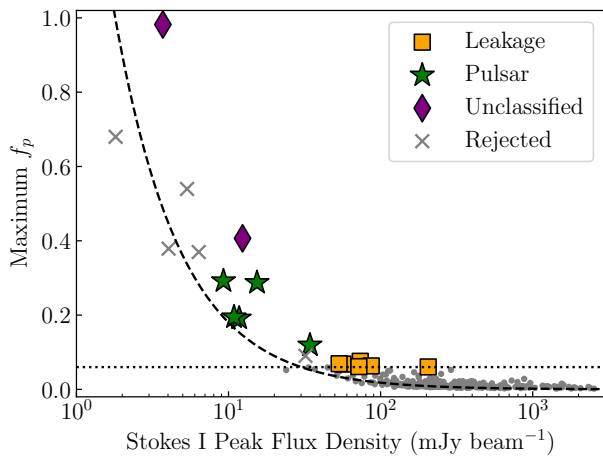


Figure 6. Maximum circular polarisation ratio of sources with respect to corresponding Stokes I flux measurements. Black dashed line shows the $5\sigma/I$, where σ is approximate noise (~ 0.36 mJy/beam) among all fields and epochs in Stokes V images. Black dotted line represents the threshold (6 per cent) we used to pick up candidates. The known pulsars found in the search are shown in green stars. Orange squares are possible leakage from bright sources. Two unclassified sources are shown in purple diamonds. Gray crosses denote the sources rejected after the manual inspection. The details of the sources are listed in Table 1.

eclipsing, 1.86 ms millisecond binary radio pulsar with a $\sim 0.5 M_{\odot}$ companion (Roberts 2011; Crawford et al. 2013). Eclipsing systems with companions in this mass range are often referred to as “redback” pulsars (Roberts 2011). The orbital period of this system is ~ 15 hr with an eclipse duration of ~ 15 per cent at 2000 MHz (about 2.25 hr, Crawford et al. 2013). We detected this source only at one of seven epochs, at a SNR of 8. We calculated the orbital phase based on the timing parameters reported in Crawford et al. (2013) and show the VAST lightcurve as a function of orbital phase in Figure 9. The timing parameters only predicts the orbital phase to an accuracy of

30 mins (~ 3 per cent of the orbit) at the time of our VAST-P1 observations. We also note that redbacks can have unpredictable orbital period variations (e.g., Bellm et al. 2016), so we can not be sure what the precise phase is. Assuming the model holds, we find that only four out of six non-detections can be explained by observations during eclipse. The eclipse duration could be longer at 888 MHz compared to 2 GHz, but even so we have a detection at an earlier phase than a non-detection, so likely there is some other reason for the variability. The remaining non-detections may arise from propagation effects such as interstellar scintillation, causing large variability (e.g., Rickett 1990). The scintillation strength $u \approx 16$ suggests a strong scattering regime (diffractive and/or refractive scintillation). Assuming a Kolmogorov spectrum (e.g., Rickett 1977), we calculated a diffractive scintillation bandwidth of $\Delta f_{\text{DISS}} \sim 3$ MHz and a scintillation timescale of ~ 15 mins at 888 MHz. Though the Δf_{DISS} is much small than the observing bandwidth ~ 288 MHz, our integration time is comparable to the scintillation timescale, so we may only be sampling a small number of “scintles” and could expect significant variability. Assuming the spectral index (~ -5) and the duty cycle (~ 10 per cent) derived from Crawford et al. (2013) remained the same, the expected flux density at VAST frequency (888 MHz) would be ~ 1 mJy. The only detection is likely to arise from scintillation, which boosts the flux density above our detection threshold.

VAST J173932.8–252108 is identified as PSR J1739–2521, a Rotating Radio Transient (RRAT) with a ~ 1.82 s period (Cui et al. 2017). RRATs are pulsars that show sporadic radio bursts with separations ranging from minutes to hours (McLaughlin et al. 2006). Cui et al. (2017) reported a burst rate of $\sim 23 \text{ hr}^{-1}$ and a mean flux density for single pulses of 49 mJy at 820 MHz. The burst fluence was measured to be ~ 3 Jy ms on average, and could reach as high as ~ 100 Jy ms. Assuming the bursts were evenly distributed in time, we would expect ~ 4 bursts in one VAST-P1 observation and therefore a mean flux density of $\lesssim 1$ mJy (based on the observed maximum fluence) in a 12-min image. However, we detected PSR J1739–2521 with a flux density of ~ 2 mJy in four separate observations, and this suggests that the bursts are not uniformly distributed in time. Cui

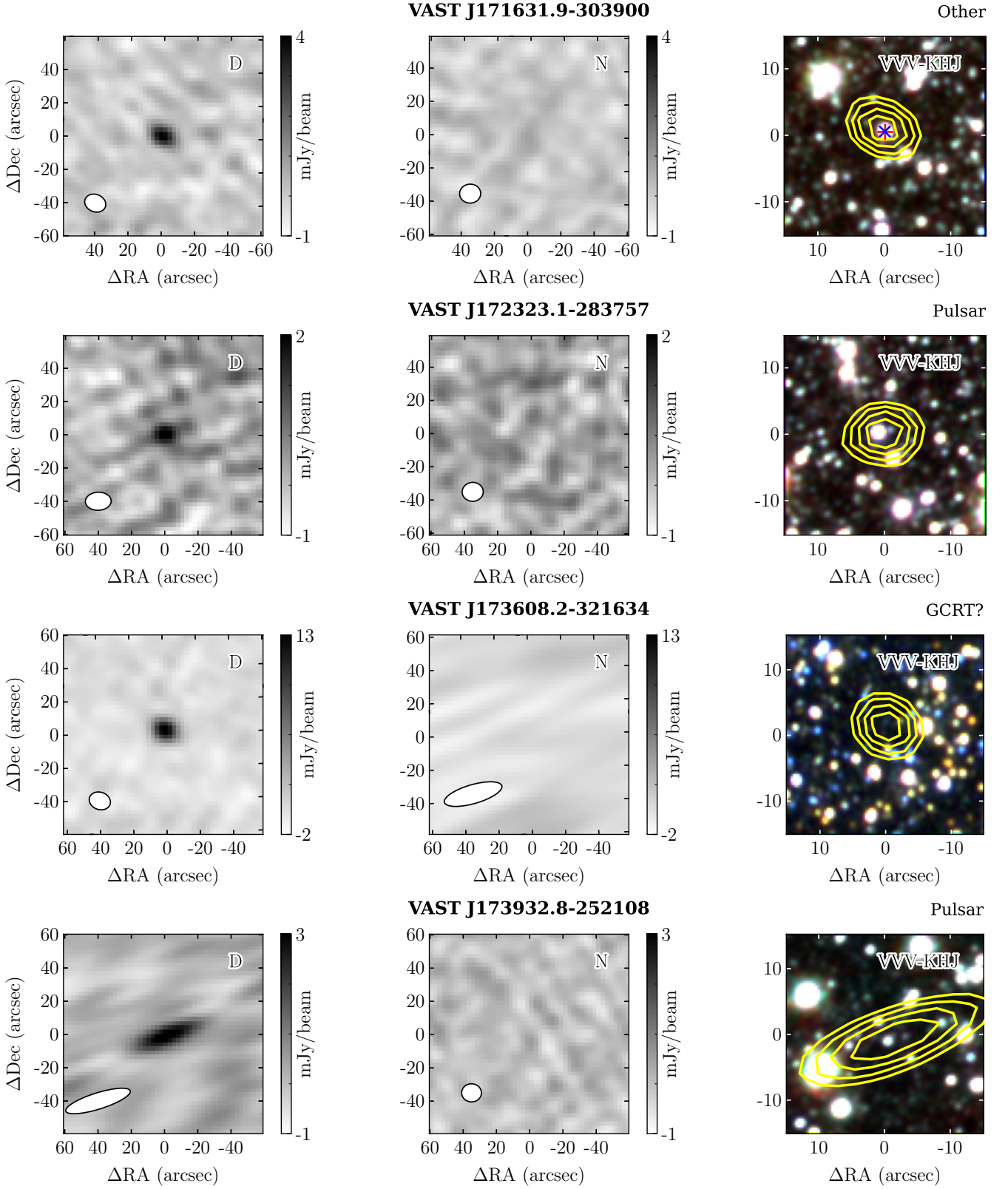


Figure 7. Images of the variable sources identified in this paper. The left panel shows the VAST Stokes I image for the epoch with the maximum flux density. The middle panel shows a non-detection epoch as a reference. The ellipse in the lower left corner of each radio image shows the FWHM of the restoring beam. The right panels show Stokes I contours at 60, 70, 80, and 90 per cent of the peak Stokes I flux density overlaid on an RGB image of infrared data from either VVV or Two Micron All Sky Survey (2MASS) with red=*K*-band, green=*H*-band, blue=*J*-band. For sources we discussed in §4.4, we also plotted their VVV and *Gaia* matches in blue \times and red $+$, respectively. All images have been centred on a frame aligned with the position of the radio source.

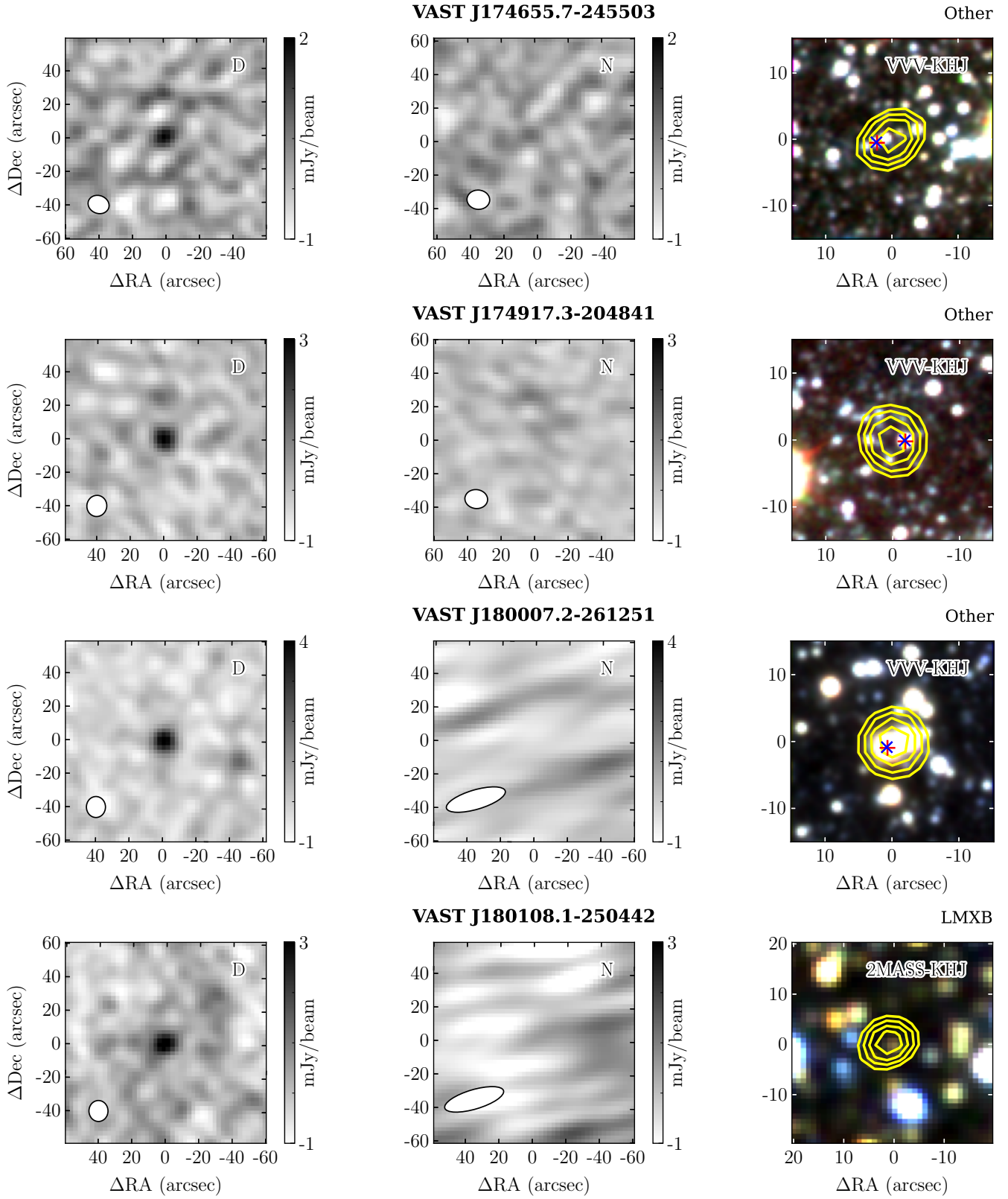


Figure 7. (continued) Images of the variable sources identified in this paper.

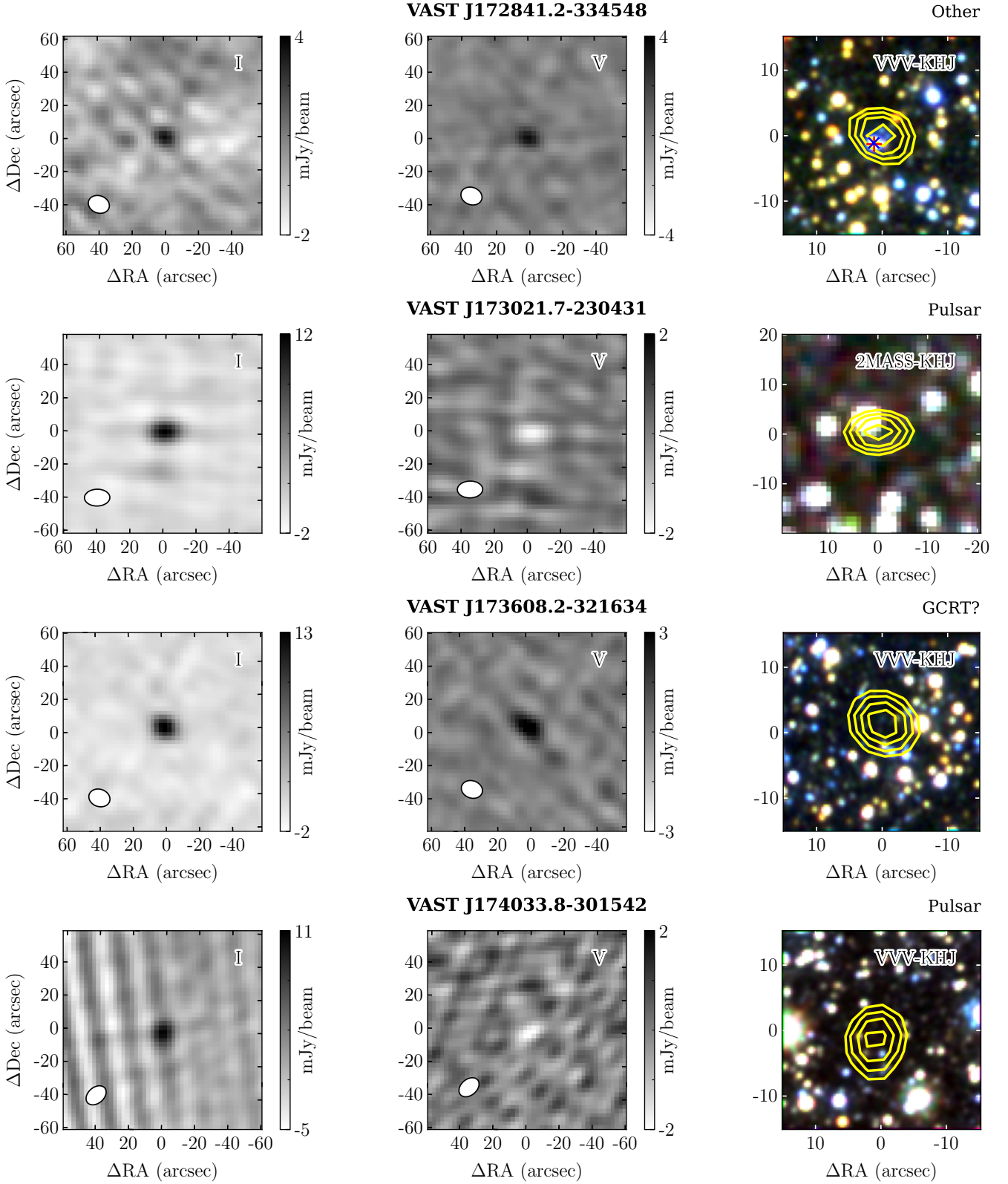


Figure 8. Images of the circularly polarised sources identified in this paper. The left panel shows the VAST Stokes I image for the epoch with the maximum flux density. The middle panel shows the Stokes V image for the same epoch where positive flux density corresponds to right handed circular polarisation and negative to left handed. The ellipse in the lower left corner of each radio image shows the FWHM of the restoring beam. The right panels show the same information as that in Figure 7. All images have been centred on a frame aligned with the position of the radio source.

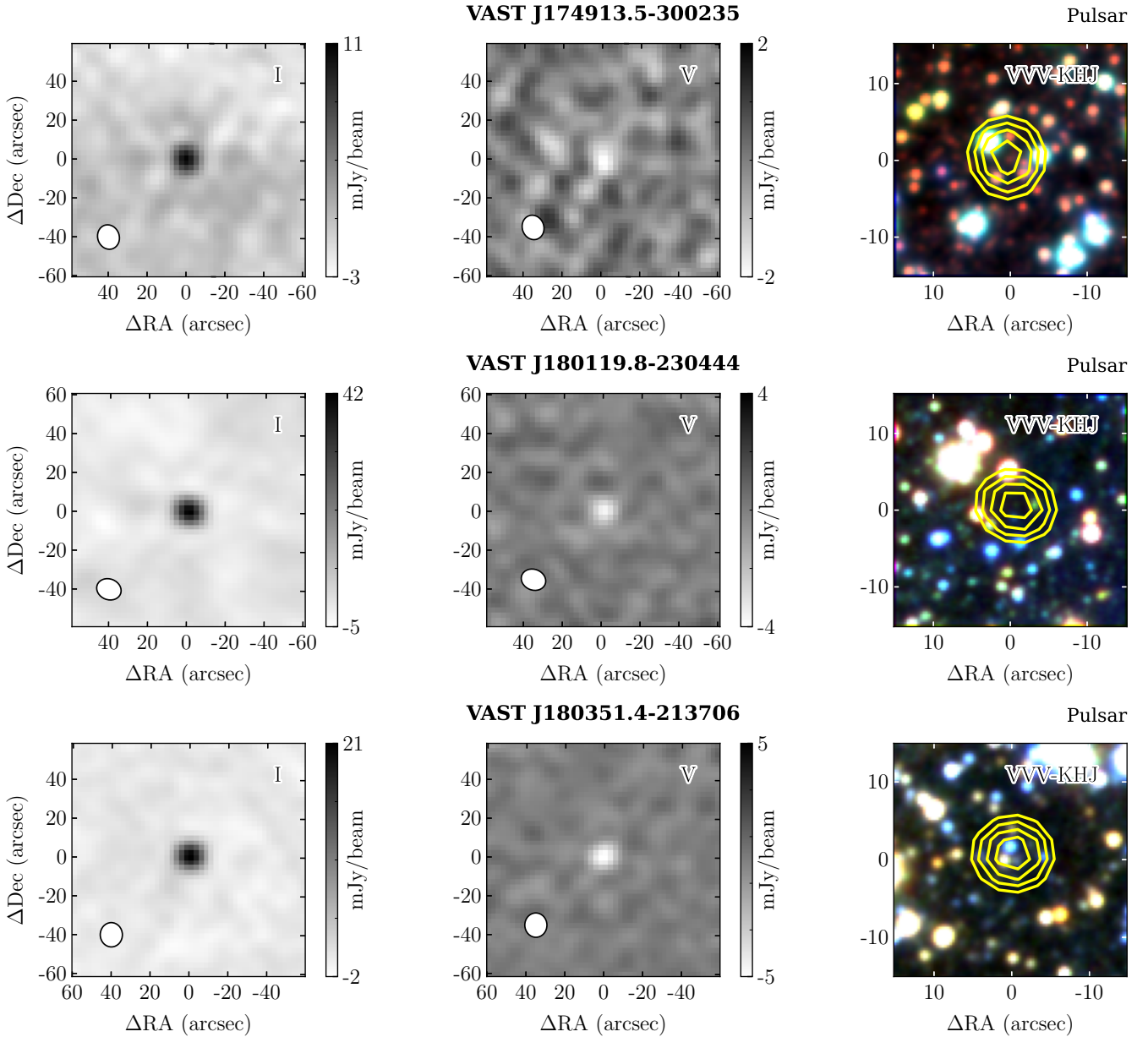


Figure 8. (continued) Images of the circularly polarised sources identified in this paper.

et al. (2017) noticed that some RRATs, including PSR J1739–2521, turned “on” and “off” regularly, with a timescale of ~ 30 min in the case of PSR J1739–2521. Therefore if one of the VAST images occurred during an “on” period, we would expect $\gg 4$ bursts and potentially a flux density consistent with what we measured (depending on the nature of the clustering). Future observations of RRATs with surveys like VAST can help determine the nature of such “on” and “off” behaviour for other sources.

4.2 Low Mass X-ray Binaries

VAST J180108.1–250442 is identified as 4U 1758–25 (1.7 arcsec offset), a Z-type LMXB (e.g., Tan *et al.* 1992). All Z-type LMXBs have been detected at radio wavelengths and show rapid variability (e.g., Tudose *et al.* 2008). For example, Tan *et al.* (1992) observed

this source with the Australia Telescope Compact Array (ATCA) for four consecutive hours, and they found that the radio emission at 4.9 GHz could be as high as ~ 5.8 mJy but could also be as low as ~ 1.7 mJy. Penninx *et al.* (1988) found that the radio emission varied as a function of the position in the X-ray colour-colour diagram, which was associated with changes in the mass accretion rate. For example, the radio flux of 4U 1758–25 was found to be lowest when the source was on horizontal branch, and highest on the normal branch (Tan *et al.* 1992). We searched for X-ray data for this source from an all sky monitoring program, the Monitor of All-sky X-ray Image (MAXI; Matsuoka *et al.* 2009)⁴. In Figure 10, we show the X-ray colour-colour diagram for 4U 1758–25 based on the data from MAXI. The source was likely on the “normal branch” when detected

⁴ <http://maxi.riken.jp/pubdata/v71/J1801-250/index.html>

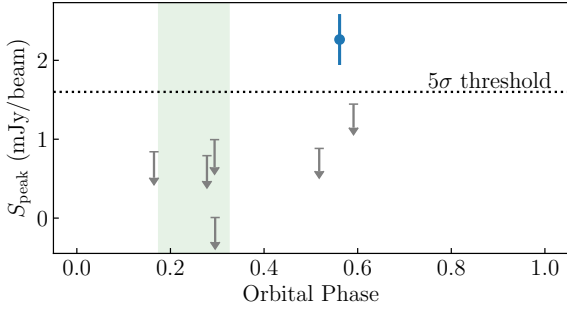


Figure 9. The VAST lightcurve for PSR J1723–2837 as a function of orbital phase (the pulsar is at inferior conjunction at a phase of 0.25). All orbital phases are calculated based on the barycentred observation times. Blue circles are peak flux density measurements from SELAVY and gray lines show the 3σ upper-limits of the forced-fitted flux density. The black dotted line shows the 5σ detection threshold towards the source position. The green shaded region shows the phases when there the pulsar is eclipsed at 2 GHz (Crawford et al. 2013): eclipses at lower frequencies like the 900-MHz data here can have longer durations (Polzin et al. 2018).

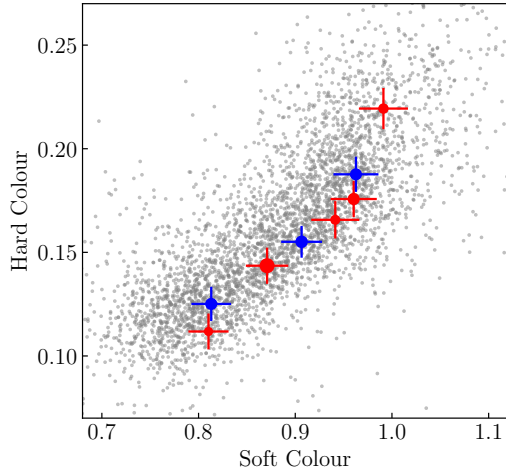


Figure 10. MAXI X-ray colour-colour diagram for 4U 1758–25. The “hard colour” is the count rate ratio for the energy channel 10–20 keV to the 4–10 keV channel; the “soft colour” is the ratio for the 4–10 keV channel to the 2–4 keV energy channel. Circles show the colours for the closest MAXI observation, where blue circles show the radio detections and red circles show the radio non-detections. The size of circles infers either the peak flux density measurements (for detections) or 3σ upper-limits of the forced-fitted flux density (for non-detections).

in VAST, which is associated with radio detections in Tan et al. (1992) and is therefore likely consistent with what we see. Future observations of a larger sample of LMXBs will help elucidate radio–X-ray state correlations of other sources.

4.3 Galactic Centre Radio Transients

Galactic Centre Radio Transients (GCRTs) are a group of unclassified radio sources located towards the Galactic centre. There are three GCRTs detected so far: GCRT J1746–2757 (Hyman et al. 2002), GCRT J1745–3009 (Hyman et al. 2005) and GCRT J1742–3001 (Hyman et al. 2009). We identified one highly variable source likely to be a new GCRT, which was published separately by Wang et al. (2021). We summarize the results from that work here.

VAST J173608.2–321634 is not coincident with any source at other wavelengths within the surveys we searched. The flux density of the source varied more than a factor of ~ 10 over timescales of months. The source was also detected to be circularly polarised (up to 41 per cent). Pulsars are commonly variable in the radio and show circular polarisation. We therefore searched for pulsations with the Parkes telescope (Murriyang) but found nothing. Later, we used the MeerKAT telescope to perform simultaneous imaging and pulsar searching observations. We did not find any pulsations but measured the flux density declining exponentially with a timescale of a day. We calculated the spectral index within the bandpass to be ~ -3 . Both this source and GCRTs are highly polarised and with steep spectra. Overall we could not classify this source as a star, pulsar or other source type, and so its most likely classification is as a GCRT.

We also performed a targeted search for radio emission from the other known GCRTs. The estimated flux density at 887.5 MHz of the burst can reach ~ 10 mJy in one 12-min VAST observation (assuming the burst with a peak flux density of ~ 1 Jy at 330 MHz with a ~ 10 min duration and a spectral index of ~ -4), which can be easily detected ($\sim 20\sigma$) in the VAST-P1. However, there is no detection from any of these three GCRTs (GCRT J1746–2757, GCRT J1745–3009, and GCRT J1742–3001) with a 5σ upper limit of ~ 5 mJy (see details in Table 4). There are two possible interpretations: (1) the GCRTs were “off” in all observations; (2) the spectral index was steeper than that we used to estimate expected flux densities, for example, Hyman et al. (2007) detected a steep-spectrum burst from GCRT J1745–3009 with a spectral index of -13.5 (this would give us an estimated flux density at 887.5 MHz of $\sim 1 \mu\text{Jy}$). Regardless, further VAST observations once the full survey commences will be useful to investigate these sources. Future observations may give us insight into the behaviour of GCRTs at higher frequencies and perhaps find new GCRTs towards the Galactic Centre.

4.4 Other sources

The remaining four highly variable sources and one highly polarised source were not associated with a previously identified pulsar or star. In order to get better positions, we observed these five candidates with the ATCA for 6–10 hours at 2.1 GHz. The observation details are listed in Table 2. The typical positional uncertainty for the VAST survey is ~ 1 arcsec (see Murphy et al. 2021, for example), while for our ATCA follow up observations is ~ 0.3 arcsec (assuming the configuration with the lowest resolution we used, 1.5A). In the ATCA follow-up observations, we only detected three out of five candidates (see the discussion below). As ATCA has a better positional accuracy, we will use ATCA positions to find any multi-wavelength counterparts for these three candidates in the following discussion. In Table 3, we summarise the possible optical (*Gaia*) and infrared (VVV) counterparts for each candidates, and calculated the false association rate (FAR) for each potential counterpart to quantify the possibility of spurious associations. The *Gaia* and VVV source in the same row are likely the same source, as the separation between *Gaia* source and VVV source is small ($\lesssim 0.6$ arcsec) and the positions of nearby sources also match. Assuming Poisson distribution for sources, the FAR for an object with an offset r and a magnitude m is given by $\text{FAR} = 1 - \exp(-\pi r^2 \sigma_{\leq m})$, where $\sigma_{\leq m}$ is the average surface density of sources brighter than m . In order to get a robust counterpart, we will only discuss the source with an FAR for VVV < 5 per cent in detail in the following section. FAR relies on the catalogue completeness, but the completeness for catalogues is lower for crowded regions than other region. The average star density in

Table 2. Details of ATCA observations. For each observation, we list its starting date, central frequency, integration time, project code, and antenna configuration.

Source	Start Date	Central Frequency (MHz)	Time (min)	Project Code	Configuration
VAST J171631.9–303900	2021-12-23	2100	725	C3363	1.5A
VAST J172841.2–334548	2021-04-25	2100	160	C3431	6D
	2021-06-04	2100	240	C3431	6B
	2021-09-11	2100	300	C3431	6A
	2021-12-24	2100	820	C3363	1.5A
VAST J174655.7–245503	2021-12-25	2100	860	C3363	1.5A
VAST J174917.3–204841	2020-11-15	2100	530	C3363	6B
	2021-12-26	2100	780	C3363	1.5A
VAST J180007.2–261251	2020-11-14	2100	510	C3363	6B

Gaia near our candidates is $\sim 8 \times 10^5 \text{ deg}^{-2}$. Fabricius et al. (2021) reported that the completeness of *Gaia* EDR3 catalogue for crowded (star density ranges from 5×10^5 to $2 \times 10^6 \text{ deg}^{-2}$) regions is ~ 20 per cent lower than the uncrowded (star density less than $5 \times 10^5 \text{ deg}^{-2}$) ones. To the magnitude limit for our candidates (~ 14 mag in K_s -band), the completeness for VVV catalogue is higher than *Gaia* (see e.g., Surot et al. 2019), though the completeness towards the Galactic Bulge is still lower than that for other uncrowded regions. A low completeness means an underestimate of $\sigma_{\leq m}$, which then leads to an underestimate of the FAR.

VAST J171631.9–303900 was detected in our ATCA follow-up observations. We observed this source for 10 hrs and detected a source at RA = 17:16:31.96±0.01, Dec = –30:39:01.38±0.61 with a peak flux density of 0.44±0.04 mJy at 2.1 GHz (see Figure 11). This source may be coincident with the optical counterpart, *Gaia* 5980701312115439616 with a magnitude $G = 17.12$ and a colour $G - G_{RP} = 1.14$, and the infrared counterpart, VVV J171631.92–303859.91 with a magnitude $K_s = 12.97$ and a colour $J - K_s = 1.04$. We can use a distance-independent colour $G - G_{RP}$ (see e.g., Andrae et al. 2018) and typical intrinsic colour and magnitude for dwarfs stellar object (Pecaut & Mamajek 2013)⁵ to infer the source properties. The *Gaia* colour implies an effective temperature of 3500 K or so (i.e., spectral type of M or so). If this object is a dwarf star, the absolute magnitude in G -band would be 11 mag or so, which implies the distance to the source is about 160 pc (consistent with that derived from the VVV magnitude). The corresponding radio luminosity is $\sim 10^{17} \text{ erg Hz}^{-1} \text{ s}^{-1}$, which is consistent with that for typical dwarf stars (e.g., Wendker 1995). The parallax for such a distance (~ 5 mas) would be easily detected by *Gaia*, but no parallax detected with a 5σ limit of ~ 1 mas (for sources with a magnitude $G \sim 17$). However, the parallax error can reach ~ 1 mas for the worst case. Based on the VVV colour and magnitude, this source could also be an M-type giant star at a distance of ~ 2 kpc, if we using the extinction coefficients in Yuan et al. (2013) and assuming an average extinction in the visual band of $A_V/d \approx 1.8 \text{ mag kpc}^{-1}$ (Whittet 1992). Further optical or infrared follow-up could be helpful in determining the precise distance. We also identified another possible counterpart in *Gaia* DR3 but with a higher FAR (see Table 3) and we will not discuss that in details.

We note that our ATCA follow-up observation had a larger uncertainty in the declination direction. A more precise radio observation would help us to get a better astrometry. Deeper optical and/or infrared observations are also needed to determine which (if either) infrared source is the counterpart of the radio source and help elucidate the nature of the source.

VAST J172841.2–334548 was not detected (with a 3σ upper

limit of $< 150 \mu\text{Jy}$) in our ATCA follow-up observations for this candidate. We combined all four ATCA follow-up observations and derived a 3σ upper limit of the quiescent radio emission of $< 90 \mu\text{Jy}$ (see Figure 12). Though the FAR for the possible *Gaia* match is less than 5 per cent, we do not think this object is a reliable counterpart as the source density for *Gaia* in this region is ~ 20 times less than that for all other candidates, but the source density for VVV is consistent. There is a probability that there is no detectable optical or infrared counterpart with *Gaia* and/or VVV sensitivity. This radio source was observed to be ~ 100 per cent circularly polarised. Sources with circular polarisation but without an obvious infrared or optical counterpart could be cool brown dwarfs (e.g., BDR J1750+3809, Vedantham et al. 2020), pulsars (Kaplan et al. 2008) or GCRTs (Roy et al. 2010). If the source is a brown dwarf with a similar radio spectral luminosity ($\sim 5 \times 10^{15} \text{ erg s}^{-1} \text{ Hz}^{-1}$, Vedantham et al. 2020) as BDR J1750+3809, the source would be at a distance of ~ 33 pc. A deeper near-infrared observation would be helpful to find the counterpart and constrain its spectral type. As noted in Johnston & Kerr (2018), very few (≤ 0.2 per cent) pulsars have fractional circular polarisation > 50 per cent. If the radio emission came from a pulsar, it could be a pulsar with unusual polarimetric properties. With a high variability, high fractional circular polarisation and no obvious optical/infrared counterpart, this source could be another GCRT. A steep radio spectrum is another characteristic of GCRTs. However, we cannot measure a reliable spectral index within the bandpass for the VAST detection due to the low detection significance. Assuming the source was radio bright with the same flux density at low frequency (887.5 MHz) when we monitored the source with ATCA, the spectral index of the source would be as high as ~ -4 . However, the spectral index estimation is likely to be wrong as the flux density is highly variable. This source was only detected once in our survey. Higher resolution and sensitivity radio monitoring observations would be beneficial in determining the emission cadence, spectral properties and other wavelength counterparts. The same strategy as VAST J173608.2–321634 can be applied to this source. For monitoring observations, simultaneous pulsar searching observations can help us confirm or rule out the pulsar origin.

VAST J174655.7–245503 was detected in our ATCA follow-up observations at RA = 17:46:55.80±0.01, Dec = –24:55:03.88±0.32 with a peak flux density of 0.70±0.04 mJy at 2.1 GHz (see Figure 11). This source appears coincident with the infrared source VVV J174655.83–245504.24 with a colour $J - K_s = 1.70$ and a magnitude $K_s = 14.23$ and the optical source *Gaia* 4068030058829222400 with a magnitude $G = 20.62$ (not detected in G_{RP}). The other object (*Gaia* 4068030024469484160 and VVV J174655.73–245503.66) nearby (see Table 3 and middle panel in Figure 11) could also be the counterpart. We did the same analysis as that for VAST J171631.9–303900. The VVV colours suggest both of them are likely to be a red giant branch stars at a distance of 1 – 2 kpc with a radio luminosity of

⁵ https://www.pas.rochester.edu/~emamajek/EEM_dwarf_UBVIJHK_colors_Teff.txt

Table 3. Highly variable and circular polarised sources with possible *Gaia* (optical) and VVV (infrared) counterparts in our search. “Best Radio Position” gives the best radio coordinate of the candidate. For each *Gaia* and VVV counterpart, we list its name (or ID), offset between our best radio position and the *Gaia* or VVV counterpart, and false association rate (FAR) for this counterpart. In following discussion, we considered the counterpart with an FAR for VVV <5 per cent as a true match.

Source	Best Radio Position	<i>Gaia</i>			VVV		
		Name	Offset (")	FAR	Name	Offset (")	FAR
VAST J171631.9–303900	17:16:31.96 –30:39:01.38	5980701316456690944	0.43	0.040
		5980701312115439616	1.48	0.023	VVV J171631.92–303859.91	1.53	0.020
VAST J172841.2–334548	17:28:41.2 –33:45:48	5975990832499505152	1.79	0.009	VVV J172841.33–334549.71	1.70	0.075
VAST J174655.7–245503	17:46:55.80 –24:55:03.88	4068030058829222400	0.59	0.037	VVV J174655.83–245504.24	0.61	0.021
		4068030024469484160	0.93	0.057	VVV J174655.73–245503.66	0.88	0.039
VAST J174917.3–204841	17:49:17.3 –20:48:41	4118772073824693504	1.90	0.040	VVV J174917.20–204841.36	1.80	0.055
VAST J180007.2–261251	18:00:07.23 –26:12:53.22	4064068277987477632	0.45	0.002	VVV J180007.24–261252.67	0.58	0.000

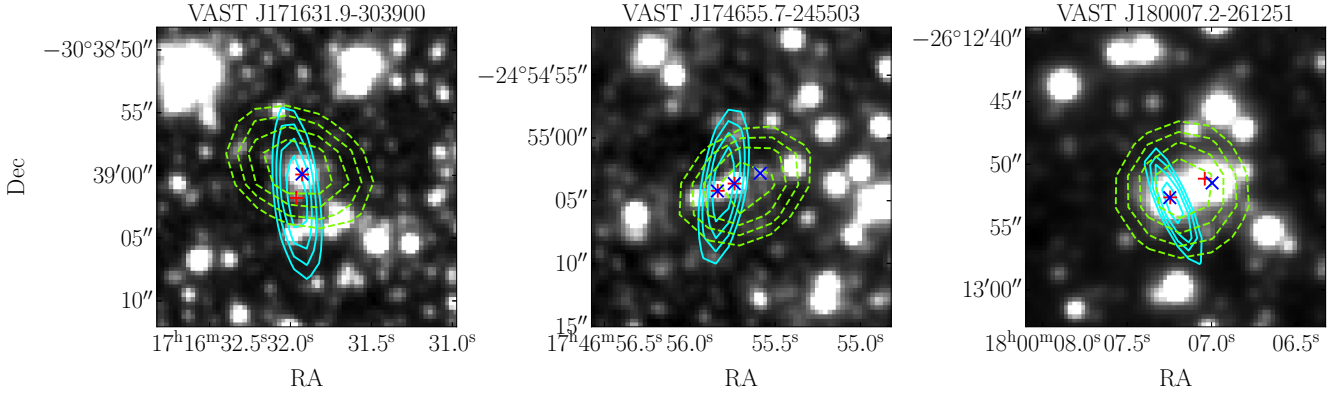


Figure 11. ASKAP (green dashed) and ATCA (cyan solid) contours at 60, 70, 80, 90 per cent of the peak Stokes I flux density overlaid on VVV *J*-band image for three of our candidates detected in ATCA follow-up observations. We also plotted VVV and *Gaia* sources nearby in blue \times and red $+$, respectively.

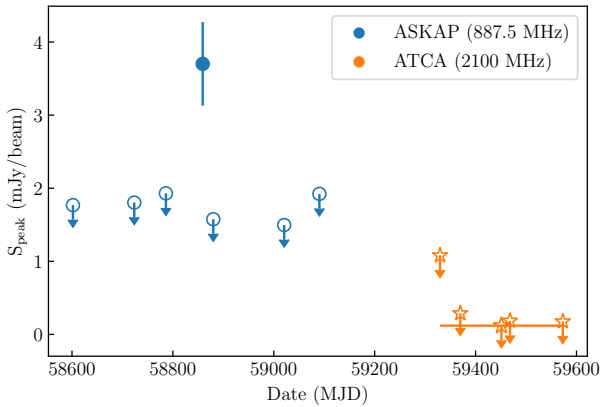


Figure 12. Full radio lightcurve for VAST J172841.2–334548. Blue circles show observations with ASKAP while orange stars show observations with ATCA.

$\sim 10^{18}$ erg Hz $^{-1}$ s $^{-1}$. A higher resolution radio observation is needed to determine which object (if either) is the counterpart.

VAST J174917.3–204841 was not detected (with a 3σ upper limit of $< 100 \mu\text{Jy}$) in our ATCA follow-up observations for this candidate. As is shown in Table 3, the FAR for possible nearby object is greater than 5 per cent and therefore we do not regard this object as a reliable counterpart. Like VAST J172841.2–334548, this source was only detected once in our survey. Higher resolution radio monitoring observations are needed for determining the source nature.

VAST J180007.2–261251 was detected in our ATCA observation at RA = 18:00:07.23 \pm 0.01, Dec = –26:12:53.22 \pm 0.17 with a peak flux of 0.94 \pm 0.03 mJy. Based on the ATCA position, we identified the infrared source VVV J180007.24–261252.67 with a colour $J - K_s = 1.14$ and a magnitude $K_s = 10.68$ as a likely counterpart. This source was also identified as *Gaia* 4064068277987477632 with a colour $G - G_{\text{RP}} = 1.74$ and a magnitude $G = 17.83$. The source was also identified as a large amplitude variable in *Gaia* DR2 with an amplitude of variation of ~ 0.3 mag in *G*-band (Mowlavi et al. 2021). The *Gaia* colour suggests the source is with an effective temperature of ~ 2500 K (i.e., spectral type of M or L). If this object is a dwarf star, the absolute magnitude in *G*-band would be approximately 16 mag, which implies the distance to the source is only about 30 pc. The parallax for such a distance (~ 30 mas) would be easily detected by *Gaia*, but no parallax detected with a 5σ limit of ~ 5 mas. However, the goodness of fit is poor and excess noise is high for this *Gaia* measurement. The infrared colour ($J - K_s = 1.14$) suggests an extinction in *V*-band of $A_V \sim 1.0$ mag (assuming a spectral type of late M). This extinction implies that the distance to the source should be around 600 pc. At such a distance, the source should be ~ 6 mag brighter than a dwarf star with the same temperature, which suggests that this object might be a giant star with a radio luminosity of $\sim 10^{18}$ erg Hz $^{-1}$ s $^{-1}$. In order to get a more reliable distance estimation and therefore work out the source nature, further optical or near infrared follow-up observations are needed.

In summary, we have searched for possible optical or infrared sources that are coincident with our radio sources. We identified three candidates as possible stellar objects. Two of them are likely to be giant stars and the remaining one might be a dwarf star. Giant

stars that are radio loud are usually found in binary systems, such as RS Canum Venaticorum systems (e.g., [Toet et al. 2021](#)) and Symbiotic stars (e.g., [Seaquist et al. 1984](#)). Radio emission from dwarf stars can arise from plasma emission or electron cyclotron maser emission (see [Dulk 1985](#) for a detailed review). However, with limited optical and infrared data, we can only discuss properties of the object semi-quantitatively based on its colours, magnitudes and distance estimations. A detailed spectroscopy infrared observation can be used to confirm the binary nature and determine the spectral type. The remaining two need further investigations such as deep optical and/or infrared observations and further radio monitoring observations, as the possible nearby optical and infrared matches are with a high FAR. Our lower limit on the flux ratio of near-IR (*J*-band) to radio (F_{radio}/F_J) is ~ 1 , which is more extreme than almost all types of stars (see Figure 7 in [Wang et al. 2022](#)). Extinction could moderate this conclusion somewhat, but is unlikely to be a major factor for most main sequence/dwarf stars (see the discussion above). This suggests that if these sources are stellar they probe the extreme end of the radio luminosity distribution which could be probed by deeper near-IR observations, or that they are another source class entirely. Deeper optical and infrared observations is useful for searching faint counterparts such as ultracool dwarfs. Higher resolution radio monitoring observations would help us to get a better astrometry, know more about the radio emission behaviors and therefore work out the origin of the transient radio emission.

4.5 Variability rates analysis

We found eight highly variable or transient sources out of 29 410 unique sources within the Galactic Centre region of VAST-P1 with a sky area of 265 deg^2 . The real number of variable or transient sources could be higher as we adopted strict variability thresholds and excluded sources with siblings or neighbours within 30 arcsec (~ 3 per cent survey area in our search). We note that the search strategy used in this paper would overlook sources in complex regions such as pulsars in supernova remnants. Different methods such as targeted search or image subtraction will work better for those cases. Only a small percentage (0.03 per cent) of sources above $\sim 2 \text{ mJy}$ are variable on a timescale of a few months. This is slightly higher than that found in other regions in VAST-P1 ([Murphy et al. 2021](#)) but overall they are both consistent with previous searches ([Mooley et al. 2016](#)).

GCRTs are steep spectra polarised radio transients towards the Galactic Centre with no clear other wavelengths counterpart ([Hyman et al. 2005](#); [Kaplan et al. 2008](#); [Roy et al. 2010](#)). We find one source, VAST J173608.2–321634 ([Wang et al. 2021](#)), which meets most of the criteria (variable, polarised, steep spectrum, and no counterpart) of the GCRTs. We find two additional sources that meet some of these criteria, but which also have not been investigated fully. For instance, VAST J172841.2–334548 is polarised, variable, and has no counterpart at other wavelengths. However, with only one detection we can not determine the lightcurve or spectral index. VAST J174917.3–204841 is variable and with no other wavelengths counterpart. Given the relative low detection significance, we cannot put a strong constraint on spectral indices and fractional circular polarisation estimation. We therefore consider these candidate GCRTs pending further investigations, which should also include deeper optical and infrared observations to determine which (if any) counterparts are plausible. That gives a total number of such unclassified sources of one to three. Other surveys have also found a few GCRT-like sources. For example, [Hyman et al. \(2021\)](#) found two steep-spectrum polarised source, C1748–2827 and C1709–3918, towards the Galactic Bulge but with no counterpart at other wave-

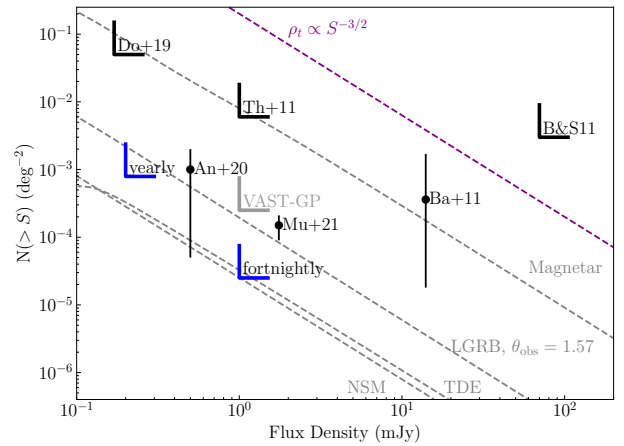


Figure 13. Two-epoch transient source surface density limits adapted from Figure 11 in [Murphy et al. \(2021\)](#). Black wedges show upper limits from previous transients search on week-month timescales ([Bower & Saul 2011](#); [Thyagarajan et al. 2011](#); [Dobie et al. 2019](#)), while black markers show rates from searches with detected transients ([Bannister et al. 2011](#); [Anderson et al. 2020](#)). Gray wedge denotes upper limit for the originally proposed VAST Galactic Plane field (VAST-GP) from [Murphy et al. \(2013\)](#). Blue wedges show the phase space accessible with updated proposed Galactic field in the full survey operations with different search cadences. The predicted rates of neutron star mergers (NSM), magnetars, long gamma ray bursts (LGRB) and tidal disruption events (TDE) from [Metzger et al. \(2015\)](#) are shown in dashed gray lines. The relation for a Euclidean source population ($\rho_t \propto S^{-3/2}$) is shown with the dashed purple line.

lengths. They were thought to be pulsar candidates but no pulsations were detected. We summarize the properties of the confirmed GCRTs and GCRT-like candidates in Table 4.

Calculating transient detection rates for GCRT-like sources can allow us to analyze the source population. We used Equation 3 in [Chiti et al. \(2016\)](#) to calculate the transient rate ρ , the number of detectable transients per unit solid angle per unit time for the highly likely GCRT, VAST J173608.2–321634. The peak flux density for this source was 12 mJy , corresponding to an rms noise threshold of 2.4 mJy for a 5σ detection threshold. The total volume of our survey Ω with $\sigma_{\text{rms}} < 2.4 \text{ mJy}$ was 592.3 hr deg^2 . We found one such transient event in the search, which gives us a rate of $\rho(n = 1, S_{\text{min}} = 12 \text{ mJy}) = 1.7^{+6.3}_{-1.6} \times 10^{-3} \text{ hr}^{-1} \text{ deg}^{-2}$ (the uncertainty was set by 95 per cent confidence intervals). The real rate should be slightly higher. Our sparse sampling would miss ~ 70 per cent of transient events that can last three weeks (we saw probably persistent emission from VAST J173608.2–321634 for about three weeks from 2020 Jan 11 to Feb 01). The event detection rate for VAST J173608.2–321634 is comparable to that derived from GCRT J1745–3009 with a rate of $3.6 \times 10^{-3} \text{ hr}^{-1} \text{ deg}^{-2}$ ([Polisensky et al. 2016](#)). If we assume our source is extragalactic (and hence distributed isotropically on the sky) we could expect to detect $\sim 5.6^{+20.8}_{-5.3}$, similar transients in Regions 3 and 4 of VAST-P1. However, no such sources were found in the search (see [Murphy et al. 2021](#)). The non-detection in this region gives an upper limit of rate of $< 2 \times 10^{-3} \text{ hr}^{-1} \text{ deg}^{-2}$ at 3σ confidence. Future programs such as the full VAST survey, will help us determine whether GCRT-like sources are distributed isotropically over the sky or mainly distributed towards the GC (see more discussions in §4.6).

Table 4. Properties of GCRTs and GCRT-like candidates. Θ gives the angular separation between the source and the GC. We also list the flux density range, variability timescale and polarisation (“C” stands for circular and “L” for linear) information for each source. α gives the radio spectral index for each source. nE gives the number of epochs that cover the source location. σ_{VAST} gives the typical rms for the region near the source in the VAST survey.

Source	Θ (deg)	Flux Density (mJy beam ⁻¹)	Variability Timescale	Polarisation	α	nE	σ_{VAST} (mJy beam ⁻¹)	Ref.
GCRT J1746–2757	~1.0	<20 – ~200 (330 MHz)	weeks to months	10	1.2	1
GCRT J1745–3009	~1.3	15 – ~2 000 (330 MHz)	minutes / repeating	<15% – ~100% C	-13 to -4	7	1.0	2,3,4,7
GCRT J1742–3001	~1.0	<5 – ~100 (235 MHz)	weeks to months	...	< -2	9	1.3	5
C1709–3918	~12.7	3.2 (618 MHz)	years to decades ^a	14% C	-3.18	1	0.8	6
C1748–2827	~0.7	0.6 (1.26 GHz)	years to decades ^a	14% C	-2.85	10	2.5	6
VAST J173608.2–321634	~4.0	<1.0 – 50 (888 MHz) <0.1 – 5.6 (1.3 GHz)	days to weeks	30% C (888 MHz) 80% L (1.3 GHz)	-5.5 to -2.6	9	0.5	8
VAST J172841.2–334548	~5.0	<1.0 – 3.5 (888 MHz)	<months	~100% C	...	7	0.6	this work
VAST J174917.3–204841	~8.0	<1.0 – 3.1 (888 MHz)	<months	<35% C	...	9	0.3	this work

^a Hyman et al. (2021) reported no evidence of significant variable behavior on any timescale and put a constraint on variability of $\lesssim 20\%$ on year-to-decade timescale. **Reference codes:** ¹Hyman et al. 2002, ²Hyman et al. 2005, ³Hyman et al. 2006, ⁴Hyman et al. 2007, ⁵Hyman et al. 2009, ⁶Hyman et al. 2021, ⁷Roy et al. 2010, ⁸Wang et al. 2021

4.6 Future Prospects

ASKAP is expected to begin full survey operations in late 2022. The VAST Galactic field region covers a Galactic latitude of $|b| < 6^\circ$ and declination $\delta < 0^\circ$, for 42 fields, 1260 deg² in total (compared to 5 fields, 265 deg² for the VAST-P1 Galactic Centre Region) and the expected cadence for Galactic fields is twice per month for four years. In Figure 13, we show the expected discovery rates for synchrotron transients in new Galactic fields. The phase space we can explore will be hugely improved. In the coming years, with the VAST full survey, we are able to detect more flare stars, cataclysmic variables, X-ray binaries, pulsars, magnetars and even some previously unknown classes of objects in our Galaxy. Detections of those unknown classes objects can help us get a more reliable rate estimation and understand their nature. We will be able to catch new outbursts from previously detected GCRTs (at least GCRT J1745–3009 and VAST 173608.2–321634 are not one-off outbursts) and potentially detect new samples of GCRTs in the full survey. Understanding their distribution would be an essential step of confirming or ruling out their origin. For example, local dwarf star models (e.g., Roy et al. 2010) would be less likely if they are not distributed isotropically. For the full VAST survey, we are able to observe ~30 000 hrs (including commensal access from other projects). If we image the data on 12 minutes intervals, we are able to detect ~2 000 bursts from GCRT-like sources assuming an isotropic distribution, and ~40 bursts assuming a Galactic distribution. The full survey will enable us to put a strong constrain on their distribution and surface density.

5 CONCLUSION

We performed an untargeted search for radio transients and circular polarised sources at 887.5 MHz using the data from RACS-low and VAST-P1 with ASKAP.

In the transient search, we found eight highly variable sources out of 29 410 sources in total. These sources included two known pulsars, one low mass X-ray binaries, three stars and two sources yet to be identified. We also discovered one GCRT-like source, whose origin is still unknown. We found an event detection rate for this source of $1.7^{+6.3}_{-1.6} \times 10^{-3} \text{ hr}^{-1} \text{ deg}^{-2}$ which is comparable with the rate for GCRT.

In the polarisation search, we found seven highly circular polarised sources out of 4 278 Stokes V detections in total. Five of them are known pulsars and one of them are the GCRT-like source we discov-

ered in the transient search. We also detected a 100 per cent circular polarised source but have not yet determined its origin.

With more observations in coming years, we will be able to find more transients towards the Galactic centre. More detections for the transients we discovered in this paper will help us get a better understanding of their origin. Further multi-wavelength follow up observations would also be beneficial in identifying their nature.

ACKNOWLEDGEMENTS

We thank Christian Wolf and Tim Bedding for useful discussions. TM acknowledges the support of the Australian Research Council through grant DP190100561. DK and AO are supported by NSF grant AST-1816492. JL and JP are supported by Australian Government Research Training Program Scholarship. Parts of this research were conducted by the Australian Research Council Centre of Excellence for Gravitational Wave Discovery (OzGrav), project number CE170100004.

This research was supported by the Sydney Informatics Hub (SIH), a core research facility at the University of Sydney. This work was also supported by software support resources awarded under the Astronomy Data and Computing Services (ADACS) Merit Allocation Program. ADACS is funded from the Astronomy National Collaborative Research Infrastructure Strategy (NCRIS) allocation provided by the Australian Government and managed by Astronomy Australia Limited (AAL).

The Australian Square Kilometre Array Pathfinder is part of the Australia Telescope National Facility which is managed by CSIRO. Operation of ASKAP is funded by the Australian Government with support from the National Collaborative Research Infrastructure Strategy. ASKAP uses the resources of the Pawsey Supercomputing Centre. Establishment of ASKAP, the Murchison Radio-astronomy Observatory and the Pawsey Supercomputing Centre are initiatives of the Australian Government, with support from the Government of Western Australia and the Science and Industry Endowment Fund. We acknowledge the Wajarri Yamatji as the traditional owners of the Murchison Radio-astronomy Observatory site. The Australia Telescope Compact Array is part of the Australia Telescope National Facility which is funded by the Australian Government for operation as a National Facility managed by CSIRO.

This research has made use of the SIMBAD database, operated at CDS, Strasbourg, France. This research has made use of MAXI data provided by RIKEN, JAXA and the MAXI team. This research

has made use of the VizieR catalogue access tool, CDS, Strasbourg, France. This research has made use of NASA's Astrophysics Data System Bibliographic Services. The acknowledgements were compiled using the Astronomy Acknowledgement Generator. This research make use of the following PYTHON package: ASTROPY (Astropy Collaboration et al. 2013, 2018), MATPLOTLIB (Hunter 2007), NUMPY (van der Walt et al. 2011; Harris et al. 2020), PANDAS (McKinney et al. 2010; Reback et al. 2022)

DATA AVAILABILITY

The ASKAP data used in this paper (RACS-low and VAST-P1) can be accessed through the CSIRO ASKAP Science Data Archive (CASDA⁶) under project codes AS110 and AS107. The ATCA data used in this paper can be accessed through the Australia Telescope Online Archive (ATOA⁷) under project codes C3363.

REFERENCES

- Anderson M. M., et al., 2020, *ApJ*, 903, 116
- Andrae R., et al., 2018, *A&A*, 616, A8
- Astropy Collaboration et al., 2013, *A&A*, 558, A33
- Astropy Collaboration et al., 2018, *AJ*, 156, 123
- Babusiaux C., et al., 2022, arXiv e-prints, p. arXiv:2206.05989
- Bannister K. W., Murphy T., Gaensler B. M., Hunstead R. W., Chatterjee S., 2011, *MNRAS*, 412, 634
- Bellm E. C., et al., 2016, *ApJ*, 816, 74
- Bower G. C., Saul D., 2011, *ApJ*, 728, L14
- Callingham J. R., et al., 2021, *Nature Astronomy*, 5, 1233
- Chiti A., Chatterjee S., Wharton R., Cordes J., Lazio T. J. W., Kaplan D. L., Bower G. C., Croft S., 2016, *ApJ*, 833, 11
- Condon J. J., Cotton W. D., Greisen E. W., Yin Q. F., Perley R. A., Taylor G. B., Broderick J. J., 1998, *AJ*, 115, 1693
- Cornwell T., Humphreys B., Lenc E., Voronkov M., Whiting M., Mitchell D., Ord S., Collins D., 2016, ASKAP Science Processing, ASKAP Science Case Memo Series 027, <https://www.atnf.csiro.au/projects/askap/ASKAP-SW-0020.pdf>
- Crawford F., et al., 2013, *ApJ*, 776, 20
- Cui B. Y., Boyles J., McLaughlin M. A., Palliyaguru N., 2017, *ApJ*, 840, 5
- Cutri R. M., et al. 2012, VizieR Online Data Catalog, p. II/311
- Dobie D., et al., 2019, *ApJ*, 887, L13
- Dulk G. A., 1985, *ARA&A*, 23, 169
- Fabricius C., et al., 2021, *A&A*, 649, A5
- Fender R., Stewart A., Macquart J. P., Donnarumma I., Murphy T., Deller A., Paragi Z., Chatterjee S., 2015, in *Advancing Astrophysics with the Square Kilometre Array (ASKA14)*. p. 51 (arXiv:1507.00729)
- Guzman J., et al., 2019, ASKAPsoft: ASKAP science data processor software (ascl:1912.003), <http://ascl.net/1912.003>
- Hale C. L., et al., 2021, *Publ. Astron. Soc. Australia*, 38, e058
- Harris C. R., et al., 2020, *Nature*, 585, 357
- Hotan A. W., et al., 2021, *Publ. Astron. Soc. Australia*, 38, e009
- Hunter J. D., 2007, *Computing in Science and Engineering*, 9, 90
- Hurley-Walker N., et al., 2017, *MNRAS*, 464, 1146
- Hyman S. D., Lazio T. J. W., Kassim N. E., Bartleson A. L., 2002, *AJ*, 123, 1497
- Hyman S. D., Lazio T. J. W., Kassim N. E., Nord M. E., Neureuther J. L., 2003, *Astronomische Nachrichten Supplement*, 324, 79
- Hyman S. D., Lazio T. J. W., Kassim N. E., Ray P. S., Markwardt C. B., Yusef-Zadeh F., 2005, *Nature*, 434, 50
- Hyman S. D., Lazio T. J. W., Roy S., Ray P. S., Kassim N. E., Neureuther J. L., 2006, *ApJ*, 639, 348
- Hyman S. D., Roy S., Pal S., Lazio T. J. W., Ray P. S., Kassim N. E., Bhatnagar S., 2007, *ApJ*, 660, L121
- Hyman S. D., Wijnands R., Lazio T. J. W., Pal S., Starling R., Kassim N. E., Ray P. S., 2009, *ApJ*, 696, 280
- Hyman S. D., et al., 2021, *MNRAS*, 507, 3888
- Intema H. T., Jagannathan P., Mooley K. P., Frail D. A., 2017, *A&A*, 598, A78
- Johnston S., Kerr M., 2018, *MNRAS*, 474, 4629
- Johnston S., et al., 2008, *Experimental Astronomy*, 22, 151
- Kaplan D., 2022, Pulsar Survey Scraper, doi:10.5281/zenodo.6390905, <https://doi.org/10.5281/zenodo.6390905>
- Kaplan D. L., Hyman S. D., Roy S., Bandyopadhyay R. M., Chakrabarty D., Kassim N. E., Lazio T. J. W., Ray P. S., 2008, *ApJ*, 687, 262
- Kaplan D. L., et al., 2019, *ApJ*, 884, 96
- Kassim N. E., Lazio T. J. W., Nord M., Hyman S. D., Brogan C. L., Larosa T. N., Duric N., 2003, *Astronomische Nachrichten Supplement*, 324, 65
- Lacy M., et al., 2020, *PASP*, 132, 035001
- Lenc E., Murphy T., Lynch C. R., Kaplan D. L., Zhang S. N., 2018, *MNRAS*, 478, 2835
- Lynch C. R., Lenc E., Kaplan D. L., Murphy T., Anderson G. E., 2017, *ApJ*, 836, L30
- Lyne A. G., Manchester R. N., 1988, *MNRAS*, 234, 477
- Manchester R. N., Hobbs G. B., Teoh A., Hobbs M., 2005, *AJ*, 129, 1993
- Matsuoka M., et al., 2009, *PASJ*, 61, 999
- McConnell D., et al., 2020, *Publ. Astron. Soc. Australia*, 37, e048
- McKinney W., et al., 2010, in *Proceedings of the 9th Python in Science Conference*. pp 51–56, doi:10.25080/Majora-92bf1922-00a
- McLaughlin M. A., et al., 2006, *Nature*, 439, 817
- Melrose D. B., Luo Q., 2004, *MNRAS*, 352, 915
- Metzger B. D., Williams P. K. G., Berger E., 2015, *ApJ*, 806, 224
- Minniti D., et al., 2010, *New Astron.*, 15, 433
- Mooley K. P., et al., 2016, *ApJ*, 818, 105
- Mowlavi N., et al., 2021, *A&A*, 648, A44
- Muno M. P., et al., 2003, *Astronomische Nachrichten Supplement*, 324, 33
- Murphy T., Mauch T., Green A., Hunstead R. W., Piestrzynska B., Kels A. P., Sztajer P., 2007, *MNRAS*, 382, 382
- Murphy T., et al., 2013, *Publ. Astron. Soc. Australia*, 30, e006
- Murphy T., et al., 2021, *Publ. Astron. Soc. Australia*, 38, e054
- Onken C. A., et al., 2019, *Publ. Astron. Soc. Australia*, 36, e033
- Pecaat M. J., Mamajek E. E., 2013, *ApJS*, 208, 9
- Penninx W., Lewin W. H. G., Zijlstra A. A., Mitsuda K., van Paradijs J., 1988, *Nature*, 336, 146
- Pintaldi S., Stewart A., O'Brien A., Kaplan D., Murphy T., 2021, arXiv e-prints, p. arXiv:2101.05898
- Polisensky E., et al., 2016, *ApJ*, 832, 60
- Polzin E. J., et al., 2018, *MNRAS*, 476, 1968
- Pritchard J., et al., 2021, *MNRAS*, 502, 5438
- Radhakrishnan V., Rankin J. M., 1990, *ApJ*, 352, 258
- Reback J., et al., 2022, pandas-dev/pandas: Pandas 1.4.3, doi:10.5281/zenodo.6702671, <https://doi.org/10.5281/zenodo.6702671>
- Rickett B. J., 1977, *ARA&A*, 15, 479
- Rickett B. J., 1990, *ARA&A*, 28, 561
- Roberts M. S. E., 2011, in Burgay M., D'Amico N., Esposito P., Pellizzoni A., Possenti A., eds, *American Institute of Physics Conference Series Vol. 1357, Radio Pulsars: An Astrophysical Key to Unlock the Secrets of the Universe*. pp 127–130 (arXiv:1103.0819), doi:10.1063/1.3615095
- Rowlinson A., et al., 2019, *Astronomy and Computing*, 27, 111
- Roy S., Hyman S. D., Pal S., Lazio T. J. W., Ray P. S., Kassim N. E., 2010, *ApJ*, 712, L5
- Seaquist E. R., Taylor A. R., Button S., 1984, *ApJ*, 284, 202
- Skinner G. K., 1993, *A&AS*, 97, 149
- Skrutskie M. F., et al., 2006, *AJ*, 131, 1163
- Surot F., et al., 2019, *A&A*, 629, A1
- Tan J., Lewin W. H. G., Hjellming R. M., Penninx W., van Paradijs J., van der Klis M., Mitsuda K., 1992, *ApJ*, 385, 314
- Thyagarajan N., Helfand D. J., White R. L., Becker R. H., 2011, *ApJ*, 742, 49

⁶ <https://data.csiro.au/dap/public/casda/casdaSearch.zul>

⁷ <https://atoa.atnf.csiro.au/query.jsp>

- Toet S. E. B., Vedantham H. K., Callingham J. R., Veken K. C., Shimwell T. W., Zarka P., Röttgering H. J. A., Drabent A., 2021, *A&A*, **654**, A21
- Tudose V., Fender R. P., Tzioumis A. K., Spencer R. E., van der Klis M., 2008, *MNRAS*, **390**, 447
- Vedantham H. K., et al., 2020, *ApJ*, **903**, L33
- Wang Z., et al., 2021, *ApJ*, **920**, 45
- Wang Y., et al., 2022, *ApJ*, **930**, 38
- Wayth R. B., et al., 2015, *Publ. Astron. Soc. Australia*, **32**, e025
- Wendker H. J., 1995, *A&AS*, **109**, 177
- Whiting M., Humphreys B., 2012, *Publ. Astron. Soc. Australia*, **29**, 371
- Whittet D. C. B., 1992, *Dust in the galactic environment*. (Bristol: A. Hilger)
- Wolf C., et al., 2018, *Publ. Astron. Soc. Australia*, **35**, e010
- Yuan H. B., Liu X. W., Xiang M. S., 2013, *MNRAS*, **430**, 2188
- Zhao J.-H., Morris M. R., Goss W. M., 2020, *ApJ*, **905**, 173
- van der Walt S., Colbert S. C., Varoquaux G., 2011, *Computing in Science and Engineering*, **13**, 22

APPENDIX A: HIGH FALSE ALARM RATE COUNTERPARTS IDENTIFICATION

In § 4.4, we only discussed counterparts with FAR for VVV less than 5 per cent. We perform the same analysis as what we did for VAST J171631.9–303900 and identify the possible types of nearby objects in Table 3 with high FAR.

VAST J172841.2–334548 may be coincident with the infrared source VVV J172841.33–334549.71 with a colour $J - K_s = 0.98$ and a magnitude $K_s = 13.54$ and with the optical source *Gaia* 5975990832499505152 with a colour $G - G_{RP} = 1.40$ and a magnitude $G = 18.25$. The *Gaia* colour implies an effective temperature of 3000 K or so (i.e., spectral type of M or so). This object could be a M-type dwarf at a distance of ~ 100 pc. Though there is no parallax detection in *Gaia*, the bad goodness of fit and the high significance of excess noise make parallax uncertainty unreliable. Without a more precise astrometry measurement, we cannot rule out this possibility.

VAST J174917.3–204841 is coincident with the infrared source VVV J174917.20–204841.36 with a colour $(J - K_s) = 0.92$ and a magnitude $K_s = 13.34$. This source was also identified as *Gaia* 4118772073824693504 with a colour $G - G_{RP} = 1.03$ and a magnitude $G = 17.00$. The *Gaia* colour implies an effective temperature of 4000 K or so (i.e., spectral type around K and M). This object could be a M-type dwarf at a distance of ~ 50 pc or a giant star at 2–3 kpc. Again, a dwarf origin is unlikely as *Gaia* did not detect significant parallax for this object.

This paper has been typeset from a $\text{\TeX}/\text{\LaTeX}$ file prepared by the author.